Phase transition hysteresis and anomalous Curie–Weiss behavior of ferroelectric tetragonal tungsten bronzes $Ba_2RETi_2Nb_3O_{15}$: RE=Nd, Sm

Marta Prades,[1] Héctor Beltrán,[1,a)] Nahum Masó,[1,2] Eloisa Cordoncillo,[1] and Anthony R. West[2]

[1]*Departamento de Química Inorgánica y Orgánica, Universitat Jaume I, Avda. Sos Baynat s/n, 12071 Castellón, Spain*

[2]*Department of Engineering Materials, The University of Sheffield, Mappin Street, Sheffield S1 3JD, United Kingdom*

(Received 8 July 2008; accepted 6 October 2008; published online 26 November 2008)

The ferroelectric tetragonal tungsten bronze (TTB) phases, $Ba_2RETi_2Nb_3O_{15}$:RE=Nd, Sm, were prepared by low temperature solvothermal synthesis. The permittivity versus temperature data of sintered ceramics show two unusual features: first, a hysteresis of 50–100 °C between values of the Curie temperature T_c on heat-cool cycles and second: a huge depression in the Curie–Weiss temperature T_0. Both effects are attributed to the complex nature of their TTB-related crystal structures with different superstructures above and below T_c and the difficulty in nucleating ferroelectric domains on cooling through T_c. Several factors may contribute to the latter difficulty: first, the structures contain two sets of crystallographic sites for the "active" Ti, Nb ions; second, the distribution of Ti and Nb over these two sets of sites is not random but partially ordered; and third, below T_c a weak commensurate superstructure perpendicular to the polar $\underline{c}$ axis is present, but above T_c a weak incommensurate superstructure in a similar orientation is present. Hence the formation of the ferroelectric structure on cooling requires both nucleation of polar domains involving two sets of cation sites and structural change from an incommensurate to a commensurate supercell.
 [DOI: 10.1063/1.3021460]

I. INTRODUCTION

A new family of tetragonal tungsten bronze (TTB)-structured phases of general formula $Ba_2RETi_2Nb_3O_{15}$ has been reported, which includes the larger rare earth (RE) ions ranging from La to Dy, as well as Bi, and for which less-studied Ta analogs also exist.[1–8] All members of this family exhibit ferroelectric to paraelectric transitions on heating. For the La and Bi members, relaxor behavior is observed and, for RE=La, the temperature of the permittivity maximum increases with frequency from 185 K at 100 Hz to 300 K at 1 GHz. As the size of the RE cation decreases, two effects are seen: first, the transition temperature increases and reaches 590 K for RE=Gd and second, the nature of the phase transition changes from relaxor to first order.

Structural studies using neutron diffraction data have been reported for the La analog at 100 and 400 K.[4] These studies were based on the standard tetragonal TTB unit cell, $a_0 \sim 12.4$ Å, $c_0 \sim 4$ Å, although subsequent electron diffraction studies showed a weak supercell to be present. At 100 K, the structure of the subcell has the polar space group $P4bm$ in which Ba (sites $4g$) and La (sites $2a$) are fully ordered on the large A sites, whereas Ti and Nb are partially disordered over two sets of octahedral B sites in which Nb shows a preference for site 2 ($8j$) and Ti shows a preference for site 1 ($2c$). In both sets of octahedral sites, Ti and Nb are displaced off the site centers, although it was not possible to determine whether, for a given set of sites, they are displaced equally. At 400 K, the structure of the subcell has the centrosymmetric space group $P4/mbm$ and coordinated off-center displacements of the octahedral cations are no longer apparent.[4]

Subsequent selected area electron diffraction (SAED) studies showed a complex weak superstructure, which is characterized by a doubling of the c axis, as well as the formation of a superstructure in the ab plane[5] whose nature varies from incommensurate (IC) (type 1) in the [110] direction for RE=La, Bi to commensurate (type 2) in the same direction for the smaller RE analogs: RE=Nd, Gd, Sm.

The type 2 commensurate supercell has space group $Ima2$ with cell dimensions described by the wave vectors $q_1=\frac{1}{2}(a_0^*+b_0^*)$; $q_2=\frac{1}{2}c_0^*$ (asterisk indicates reciprocal space). The type 1 IC supercell is described by the wave vectors $q_1=(\frac{1}{4}+\delta)(a_0^*+b_0^*)$; $q_2=\frac{1}{2}c_0^*$. A similar IC supercell has been observed in other TTB phases, e.g., $Ba_2NaNb_5O_{15}$ (Refs. 9 and 10) and $Ba_xSr_{1-x}Nb_2O_6$.[11–13] The origin of the modulations in the two superstructures appears to be different and the type 2 case is not simply a lock-in version of type 1.[8] Both superstructures involve coordinated tilting of octahedra but with different tilting topologies. The type 2 structure is suggested to have a single tilting pattern but with antiphase rotations of octahedra in successive layers along the $\underline{c}$ axis. In the type 1 structure, two distinct tilting configurations are proposed but without antiphase tilting about the $\underline{c}$ axis.[8]

A detailed study of the temperature dependence of SAED for RE=Nd showed a complex sequence of changes.[8] Below T_c, 400 K, the $Ima2$ supercell is observed and the structure is type 2. Above T_c, the structure is IC and type 1. At higher temperatures, the IC supercell reflections change from sharp to diffuse before disappearing completely

a)Electronic mail: mir@qio.uji.es.

≳820 K. A full structure determination of the IC phase has not been carried out; however, a similar IC structure has been found in $Ba_2NaNb_5O_{15}$ (Refs. 9 and 10) and $Ba_xSr_{1-x}Nb_2O_6$.[11–13]

SAED as a function of temperature for RE=La showed a similar sequence of transitions for the IC phase with a sharp-to-diffuse transition of the supercell reflections at ~475 K before their complete disappearance at ~725 K. For RE =La, however, there was no evidence of transition to a commensurate *Ima*2 supercell at low temperatures.

There appears to be a clear correlation between the nature of the superstructure in the *ab* plane, i.e., whether it is IC or commensurate and the relaxor/first order nature of the phase transition; intriguingly, the polar direction of the crystal structure, which appears to be responsible for the ferroelectricity, is the *c* direction perpendicular to the *ab* plane that contains the IC /commensurate supercell.

The synthesis of these TTB phases has so far been achieved by high temperature solid state reaction requiring prolonged heat treatments, e.g., 10 days at 1350 °C for hand-mixed reagents or 46 h at 1450 °C for attrition-milled samples. Products were single phased by x-ray powder diffraction (XRD), but given the unreactivity of the component oxides, the atomic-scale homogeneity of the products was not assured and indeed, there is evidence that both the Ba:RE and Ti:Nb ratios may vary, leading to possible TTB solid solution formation.[1] In addition, the detailed shape of the permittivity-temperature profile of the smaller RE members did not have the classic ferroelectric-paraelectric profile seen with, for instance, $BaTiO_3$. The initial objective of the present study was therefore to seek alternative low temperature synthesis routes based on sol-gel and solvothermal methods, so as first to avoid possible contamination during attrition milling and prolonged high temperature heat treatments, and second, to use liquid phase precursors with the possibility of achieving better atomic-scale homogeneity. Successful methods were developed for both synthesis routes; however, the phase purity of the products was higher for the solvothermal route and only those results are reported in detail here. Nevertheless, the electrical properties of the materials prepared by the two routes were essentially identical and appeared not to be influenced greatly by the presence of small amounts of secondary phases.

II. EXPERIMENTAL

$Ba(CH_3COO)_2$:99%, $Sm(C_3H_7O^i)_3$:99.9%, $Nd(C_3H_7O^i)_3$: 99.9%, $Ti(C_3H_7O^i)_4$:98%, and $Nb(OC_2H_5)_5$: > 99.9%, all Strem Chemicals, were used as starting reagents. The schemes used for sample preparation are shown in Fig. 1. De-ionized water (H_2O) and acetic acid (HAc) were used to dissolve barium acetate as detailed in Ref. 14. Solutions of barium acetate and lanthanide alkoxide were added to titanium and niobium alkoxides to give a final clear solution (sol). The Ba:H_2O:CH_3OH and RE:acacH (RE =rare earth; acacH=pentane-2,4-dione) molar ratios were 1:21:70 and 1:14, respectively. In the sol-gel method, the solvent of the final solution was evaporated and a gel was formed. For the solvothermal reaction, the final solution was

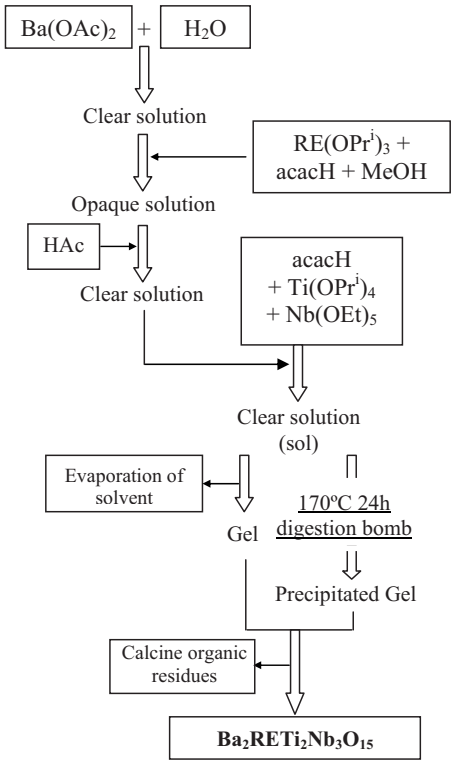

FIG. 1. Schemes used for sample preparation.

transferred to a 100 ml Teflon-lined digestion bomb, which was then heated at 170 °C for 24 h in an oven. After reaction, the resulting precipitate was separated by centrifugation and washed with acetone. In an additional experiment with the Nd analog, solvent was evaporated instead of centrifuged.

The sol-gel and solvothermal-derived powders were gradually heated to temperatures in the range of 1100–1400 °C for 12 h (sol-gel) and 2 h (solvothermal), pressed into pellets, and sintered in air at the same maximum temperature for 48 h (sol-gel) and 2 h (solvothermal), after which pellets were slow cooled inside the furnace. Product phases were identified by XRD using a Bruker D4 Endeavor diffractometer, Cu $K\alpha$ radiation.

Scanning electron micrographs (SEMs) of the pellet surfaces were taken on a SEM Leica, Leo 440 model, equipped with a spectrometer for energy dispersion of x-ray analysis using the following operation parameters: acceleration voltage 20 kV, measuring time 100 s, working distance 25 mm, counting rate 1.2 kcps. The samples for microstructure determination and microanalysis were deposited on an Al holder and coated with graphite. Differential scanning calorimetry (DSC) used a Perkin Elmer DSC7 model with heating/cooling rates 10 °C min^{-1}.

For electrical property measurements, electrodes were fabricated on opposite pellet faces from Pt paste, which was dried and decomposed by gradually heating to 900 °C. Samples with electrodes attached were placed into a conductivity jig and electrical property data recorded using an Agilent 4294A impedance analyzer over the frequency range from 40 Hz to 13 MHz and over the temperature range, room

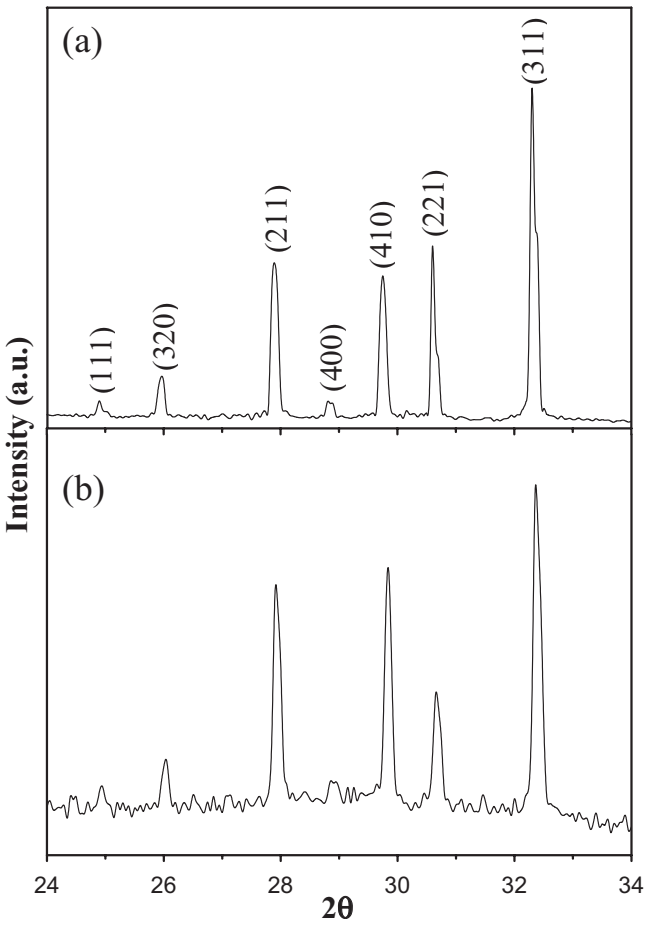

FIG. 2. XRD patterns for (a) BNTN and (b) BSTN sintered at 1300 and 1400 °C, respectively. The reflections have been indexed on the TTB subcell.

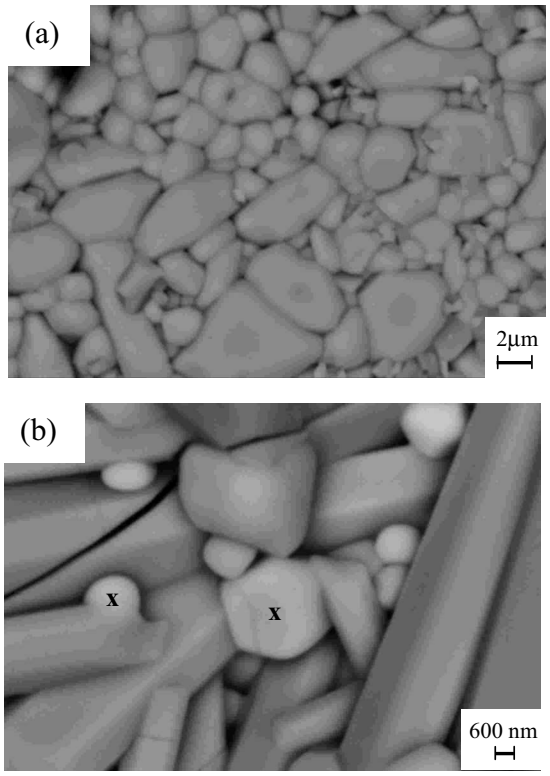

FIG. 3. SEM of the surface of (a) BNTN and (b) BSTN pellets sintered at 1300 and 1400 °C, respectively. The particles marked with a cross in (b) correspond to the secondary phase $SmNbO_4$ identified by energy dispersive x-ray analysis.

temperature to 900 °C. Impedance data were corrected for overall pellet geometry and for the blank cell capacitance ("jig correction").

III. RESULTS

The solvothermal synthesis route has been used to synthesize $Ba_2RETi_2Nb_3O_{15}$:RE=Nd (BNTN), Sm (BSTN). No difference was observed between the samples in which the solvent was separated by centrifugation or evaporated. Samples were phase pure by XRD (Fig. 2). The BNTN sample was homogeneous by SEM, whereas the BSTN sample contained a small amount of secondary phase not detected by XRD (Fig. 3). The sol-gel method with the Sm analog yielded the TTB phase as the main product but with $Ba_3Ti_4Nb_4O_{21}$ secondary phase. All of the results reported here are for samples prepared by the solvothermal route, but comments on sol-gel derived Sm samples are provided, as appropriate, for comparison.

DSC results are shown in Fig. 4. The peaks on heating are associated with the ferroelectric-paraelectric phase transitions; however, large hystereses in peak temperatures between heating and cooling are observed. The only previous report of transition hysteresis is for the Nd phase with a hysteresis of 26 K,[6] which is significantly less than that found here, ~67 K for this particular sample.

Fixed frequency electrical property data are given in Fig. 5 with data for [(a) and (b)] permittivity ε', (c) ε'^{-1}, and (d) tan δ. Pellet densities and Curie–Weiss temperatures T_0 obtained by extrapolation are given in Table I. The ε' data are shown for both heating and cooling cycles and show similar peak maximum temperatures and hystereses to those seen by DSC (Fig. 4). The permittivity data shown in (a) are for three frequencies: the overlap in the three data sets shows lack of any frequency dependence of the permittivity. The Curie–Weiss plots (c) are for the cooling cycle data; similar plots (not shown) were obtained for the heating cycle data. The Curie–Weiss temperatures T_0 are depressed so much that they are below 0 K (Table I).

The occurrence of hysteresis effects in ferroelectric materials is relatively uncommon probably because the phase transitions are displacive rather than reconstructive in nature. A series of experiments was conducted to determine which, if any, variables may influence the extent of hysteresis. The largest effect was found on varying the sintering temperature of the ceramics, as summarized in Fig. 6 for samples sintered at different temperatures. At the higher sintering temperatures, not only is the hysteresis greater between heat and cool cycles (b), but also the magnitude of the permittivity maximum is greater (a). The furnace atmosphere during sintering and also during measurement (air, oxygen, and nitrogen) had no significant effect on the electrical properties; this is not unexpected given the highly insulating nature of the samples and their insensitivity to atmospheric changes. For a given sample, the transition temperatures were fully reproducible on repeated heat-cool cycles and were independent of heat-

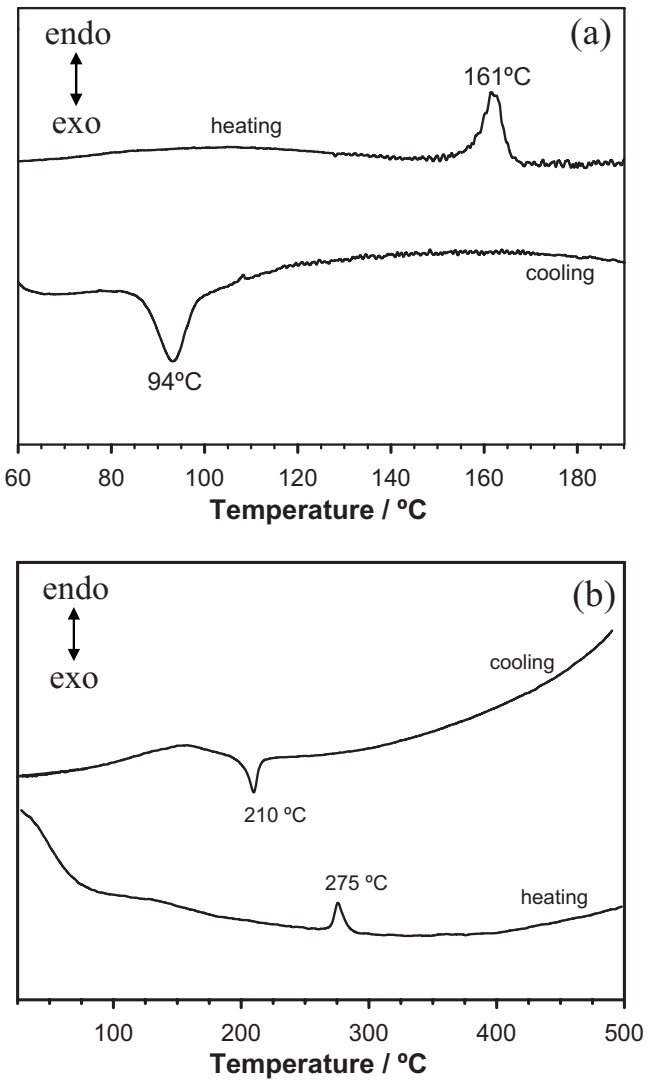

FIG. 4. DSC results for (a) BNTN and (b) BSTN samples sintered at 1100 and 1400 °C, respectively.

cool rates over the range of 2–12 °C min^{-1}. It is concluded, therefore, that the hysteresis is a real effect that depends in some way on particle size/crystallinity/homogeneity of the samples.

In order to get better insight into the electrical properties and, in particular, the electrical homogeneity of samples, variable frequency impedance measurements were carried out over a wide temperature range with a selection of typical results shown in Fig. 7. Generally, samples had a response that could be represented approximately by a single, ideal, parallel *RC* element [inset in Fig. 7(a)]. Thus, impedance complex plane plots showed an almost ideal single semicircle but with a small additional effect seen at low frequencies in the higher temperature data sets [Fig. 7(a)]. Representing the same data in the form of Z''/M'' spectroscopic plots showed single peaks in each case, which were almost coincident on the frequency scale. Since M'' spectra are dominated by low capacitance bulk effects, the data in Fig. 7(b) indicate that the main resistive component of the sample (the Z'' peak) is, in fact, the sample bulk (M'' peak).

In Fig. 7(c), the same data are presented as capacitance against frequency; a constant value is seen at high frequencies but a significant increase occurs at lower frequencies that is attributed to a thin layer effect at the sample-electrode interface. It is important, therefore, to separate bulk capacitance data from such low frequency interfacial effects in order to properly characterize and understand the intrinsic bulk properties.

The sample resistance was obtained from the low frequency intercept on the Z' axis of the impedance complex plane plots [Fig. 7(a)] and is shown in Arrhenius format in Fig. 8 for BSTN and BNTN samples. Assuming linear plots, the activation energy is ~1.49 eV; however, close inspection shows that both sets exhibit curvature with higher activation energy at higher temperature. Similar Arrhenius plots and conductivities were obtained at higher sintering temperatures (1400 °C). Figure 8 demonstrates that the samples are highly insulating, therefore, both from the high value of activation energy and the magnitude of the conductivity values, e.g., 10^{-6} S cm^{-1} at 620 °C.

Close examination of the capacitance data for samples of BNTN sintered at different temperatures (Fig. 9) shows the presence in some cases of a poorly resolved intermediate frequency capacitance plateau. The presence/absence of this plateau and its magnitude when present depended on sample sintering conditions; in particular, it was seen in samples sintered at lower temperature 1100 °C and is attributed to the ceramic microstructure, and, in particular, the presence of constriction impedances associated with grain-grain contacts and sample porosity. In well-sintered, dense samples, such effects were absent and the sample bulk capacitance is then given by the frequency-independent, high-frequency plateau. In samples containing a constriction impedance, it is possible to overestimate the sample capacitance depending on the measurement frequency that is used.

IV. DISCUSSION

The sol-gel and solvothermal methods have been used to synthesize ferroelectric TTB phases. Two steps are involved. First, soluble metal reagents are mixed to obtain a clear solution (sol); this is the same in both methods. Second, a gel is obtained after the solvent is evaporated in the sol-gel method, while for the solvothermal method, an amorphous precipitate is produced during reaction at high pressures and moderate temperatures; it is assumed that all of the reactants precipitate from solution to give the final product. In our case, there were no differences between samples in which the solvent was separated by centrifugation or evaporated, and therefore, there is no uncertainty over the precise composition of the product arising from the synthesis method.

The main results are (i) an unusually large hysteresis in phase transition temperatures and electrical properties between heat and cool cycles for two ferroelectric TTB phases, (ii) a very large depression of the Curie–Weiss temperatures T_0 compared to that usually seen for first order ferroelectric transitions, and (iii) an unusual shape of the permittivity-temperature profiles, especially above T_c. As far as we are aware, such effects, especially (ii), have not been recognized previously in ferroelectric materials.

We speculate that the origin of the hysteresis is associ-

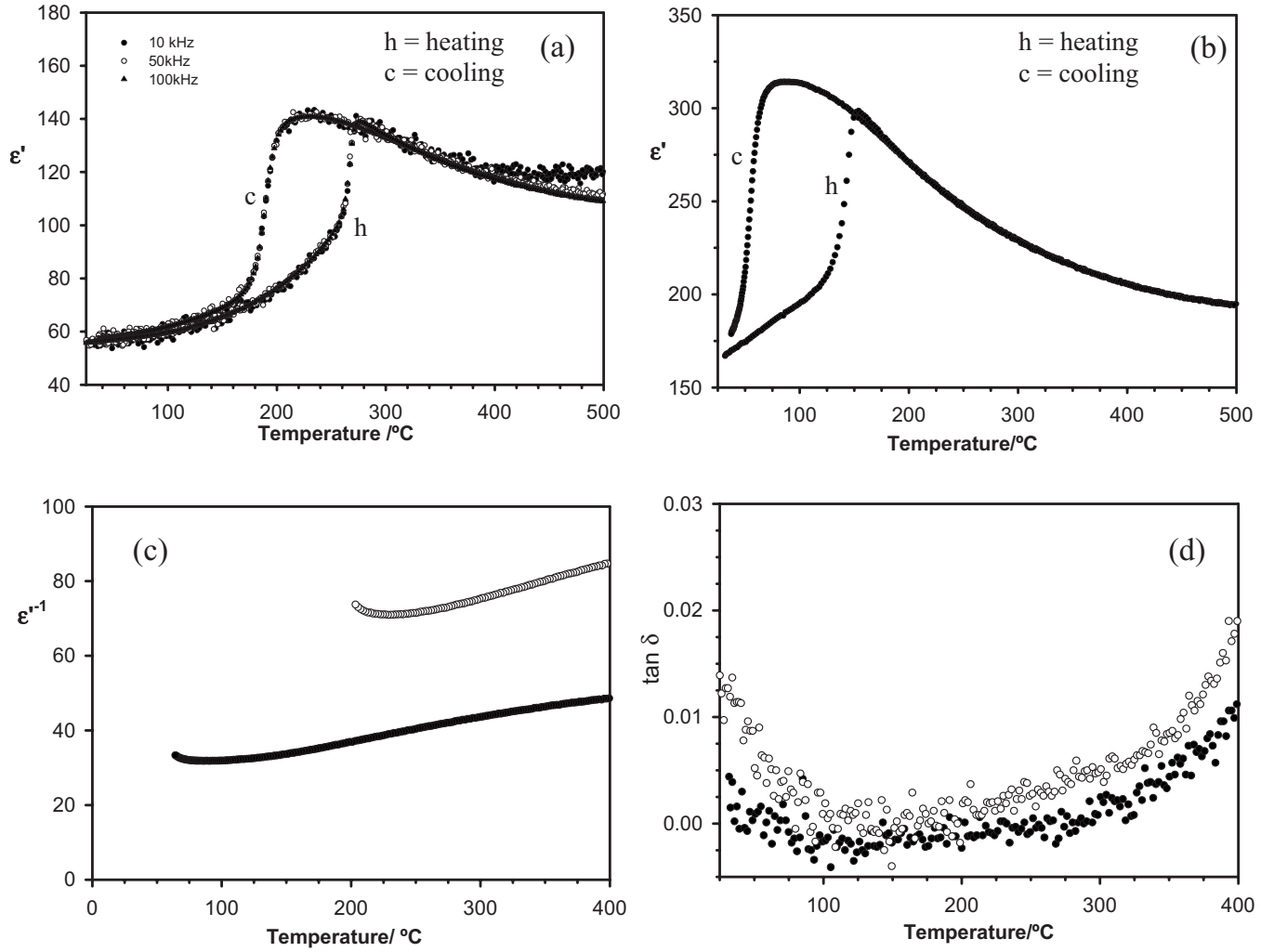

FIG. 5. (a) Permittivity ε' as a function of temperature at three different frequencies for BSTN sintered at 1400 °C and (b) at 100 kHz for BNTN sintered at 1300 °C. (c) ε'^{-1} on cool cycle and (d) tan δ for the same samples, BNTN (●) and BSTN (◯).

ated with the rather complex TTB crystal structure of the present phases. First, it contains two crystallographically distinct sets of sites for the active ions Ti and Nb. Crystallographic results from the La analog[4] showed that the distribution of Nb and Ti over the two sets of sites is not random; it is not known whether Nb and Ti are equally active in their displacement from the octahedral site center positions that are responsible for the ferroelectricity, nor whether the polar displacements occur in both sets of sites simultaneously. Second, the Nd (and probably Sm) analog has a commensurate weak superstructure below T_c, which transforms to an IC superstructure above T_c;[8] the detailed ordering responsible for the two superstructures appears to be different and the commensurate superstructure is not simply a lock-in version of the IC superstructure.

TABLE I. Density (% theoretical) and Curie–Weiss temperature T_0 of the pellets prepared.

Reference	T_{sinter} (°C)	D (%)	T_0 (°C)
BSTN	1400	76	−445
BNTN	1300	89	−319

These TTB phases are clearly not relaxor materials, unlike the RE=La,Bi analogs, since there is no variation in the permittivity maximum temperature with frequency [Fig. 5(a)]. The phase transition has first order character, as shown by the occurrence of a DSC heat effect, and the hysteresis observed on cooling may therefore be interpreted as difficulty associated with the spontaneous nucleation of ferroelectric domains on cooling. Possibly, there is more than one kind of polar defect cluster in the high-temperature paraelectric phase, given that there are two kinds of ferroelectrically active ions over two sets of crystallographic sites and, therefore, cluster reorganization may be a prerequisite to domain nucleation. Additionally, transition from the IC to the commensurate supercell on cooling may have a significant nucleation barrier since this represents a transformation between different topologies associated with tilting of $(Nb,Ti)O_6$ octahedra.

In most first order ferroelectrics, the phase transitions are essentially displacive in nature, exhibit little hysteresis on cooling, and, for instance, cannot be prevented by quenching from the high temperature paraelectric state. Significant hystereses have been reported, however, in the xPbTiO$_3$−(1−x)Bi$(Zn_{1/2}Ti_{1/2})O_3$ solid solutions and attributed to the

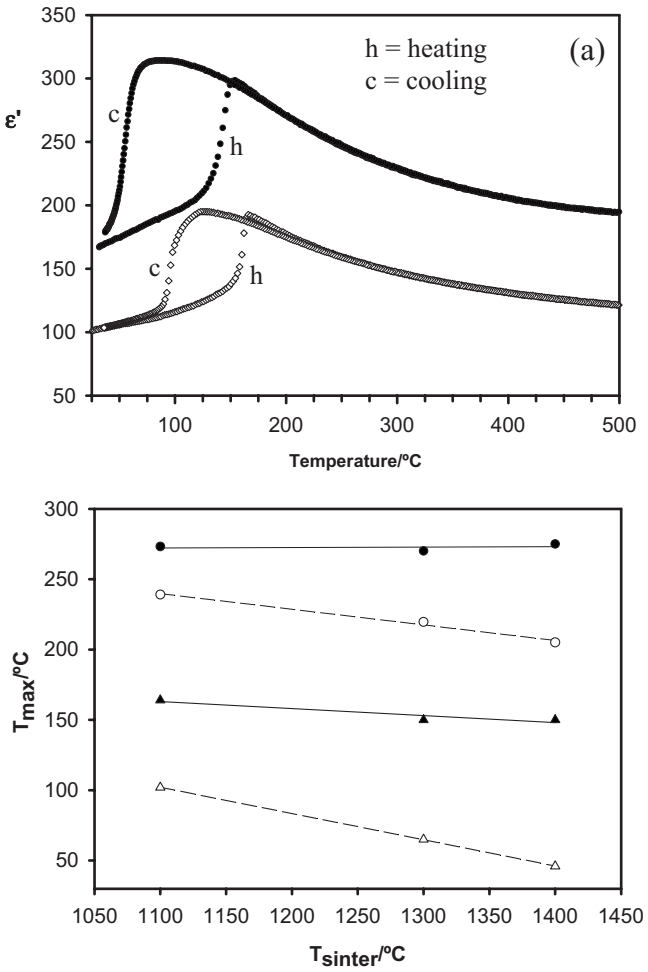

FIG. 6. (a) Permittivity ε' data as a function of temperature at 100 kHz for BNTN sintered at 1300 °C (●) and 1100 °C (◇). (b) T_{max} as a function of sintering temperature for BSTN (circles) and BNTN (triangles) samples. Data were obtained from the onset of the maximum of the peaks on heating (—) and cooling (- - - -).

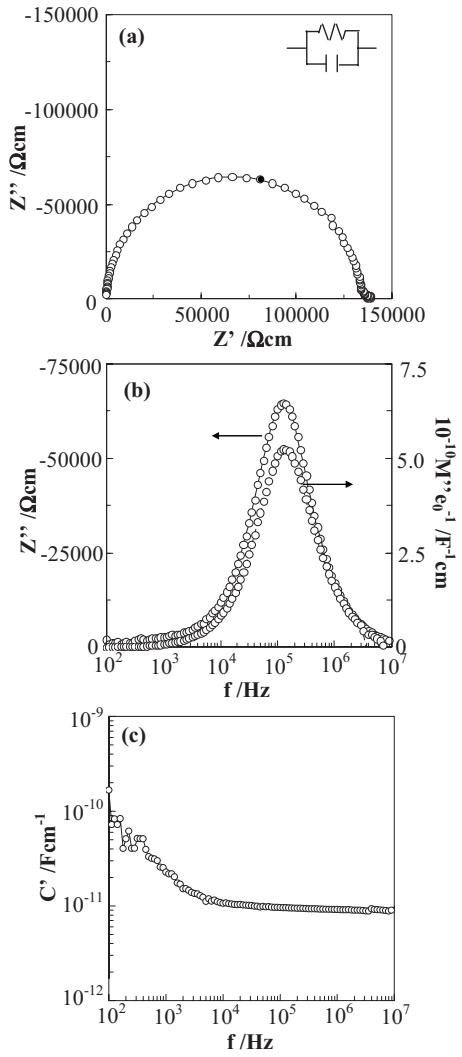

FIG. 7. (a) Impedance complex plane plot, (b) Z'' and M'' spectroscopic plots, and (c) capacitance as a function of frequency for BNTN sintered at 1300 °C. The measurements were made at 719 °C. The solid circle data point in (a) refers to a frequency of 100 kHz.

large c/a ratio in the tetragonal phase, giving rise to high strain tetragonal domains and influencing the nucleation and growth energetics.[15]

In $PbZrO_3$, a ferroelectric to antiferrolectric transition occurs at temperatures below T_c and this transition can exhibit hysteresis. Indeed, in some samples the transition can be prevented entirely and it is suggested that this occurs in samples that contain cation and oxygen vacancies arising from PbO loss during firing. In these cases, therefore, there is also a barrier to nucleation and growth of the low temperature structures during cooling.[16]

In addition to the hysteresis, an unusual feature of the electrical properties of the present phases, which appears not to have been encountered in other ferroelectric materials, is the nature of the Curie–Weiss plots, and in particular, displacement of the Curie–Weiss temperature T_0 to very low temperatures. A small difference between T_0 and the temperature of the permittivity maximum T_c is commonly observed in first order ferroelectrics such as $BaTiO_3$, whereas a much larger difference may be seen with relaxor ferroelectrics such as the difference of 100–120 °C reported for the La TTB analog (but this temperature difference depends greatly on measurement frequency). The present materials show $(T_c\text{-}T_0)$ values of several hundred degrees that are larger even than those observed for relaxors. We may again speculate on two possible origins of this effect. First, the nature of the polar clusters and the possible existence of

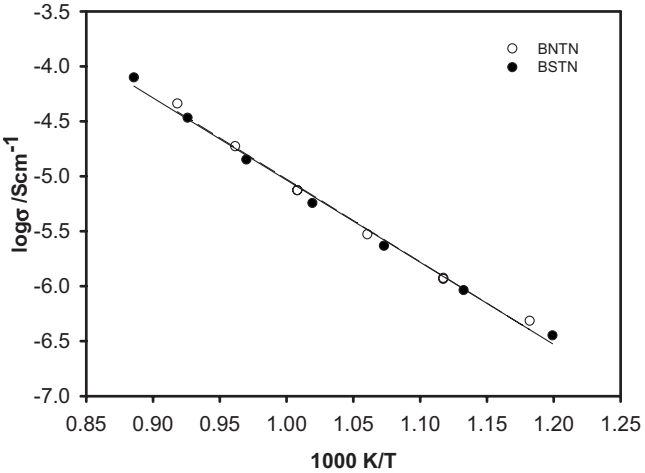

FIG. 8. Arrhenius plots of total conductivity for BNTN and BSTN samples sintered at 1300 °C.

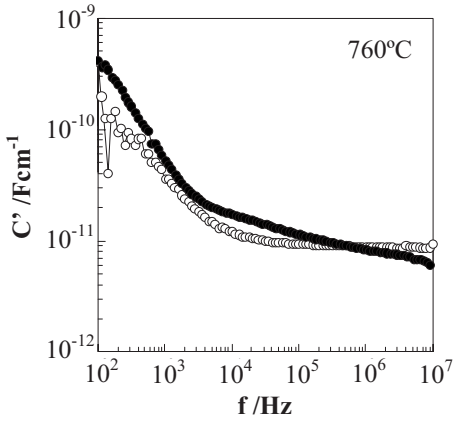

FIG. 9. Capacitance data as a function of frequency for BNTN sintered at 1300 °C (◯) and 1100 °C (●).

more than one kind of polar cluster in the paraelectric state may be responsible for the large depression of T_0. In particular, growth of dominant polar clusters on cooling toward the phase transition temperature may take place much more slowly than is expected for a first-order ferroelectric transition due to the very small difference in free energy between the different cluster configurations and, therefore, the small driving force for cluster growth. Second, it is possible that the IC phase above T_c would, in the absence of the transition to the commensurate superstructure, remain in the paraelectric state to much lower temperatures. The large reduction in T_0 may therefore reflect the intrinsic properties of the high temperature IC phase, which cannot be studied to much lower temperatures because of the intervening IC to commensurate phase transition.

It is noteworthy that the quality of the electrical property data, in particular, the permittivity data, appears to be much better for the present samples prepared by low temperature synthesis as a precursor to sintering than those prepared by direct solid state reaction at high temperatures. Although we have no direct evidence, we believe that the homogeneity of the present samples is high with good atomic scale mixing of the Ba, RE and Nb, Ti cations and that this may be responsible for the improved shapes of the permittivity profiles. The impedance data are consistent with this conclusion since they show that the electrical properties can be represented by an almost Debye-like *RC* response.

V. CONCLUSIONS

Two phases in the family of TTB ferroelectrics have been synthesized using low temperature sol-gel and solvothermal routes as an alternative to high-temperature solid state reaction, and the electrical property data, especially the permittivity-temperature profiles, are generally of much better quality. The phase purity of the solvothermal samples was better than sol-gel derived samples containing a small amount of minority phase in one case. The similarity in electrical properties of the Sm analog synthesized by both methods indicates that the final composition of each phase was similar.

Both TTB analogs, as well as the analog synthesized by two routes, exhibit significant hysteresis between heating and cooling cycles in their phase transition behavior. This is an unusual effect with ferroelectric materials. It is attributed to the complex nature of the TTB crystal structure with (a) two sets of crystallographic sites that contribute to the ferroelectricity, (b) a nonrandom distribution of two ferroelectrically active cations, Nb and Ti, over these two sets of sites, and (c) the presence of a weak superstructure that changes from IC to commensurate on cooling through T_c. This complex structure, cation distribution, and phase transition may also be responsible for the very large depression of the T_0 parameter in Curie–Weiss plots, which is very different from the behavior usually observed in first order ferroelectrics.

ACKNOWLEDGMENTS

We thank the EPSRC (A.R.W.) and "Bancaja-Universitat Jaume I" (Project No. P1 1B2006-25) (M.P., H.B., E.C.) for financial support. M.P. thanks the Generalitat Valenciana for a fellowship (Grant No. BFPI/2007/174). N.M. thanks The Worshipful Co. of Armourers and Brasiers for a travel grant.

[1] C. A. Kirk, M. C. Stennett, I. M. Reaney, and A. R. West, J. Mater. Chem. **12**, 2609 (2002).
[2] G. C. Miles, M. C. Stennett, D. Pickthall, C. A. Kirk, I. M. Reaney, and A. R. West, Powder Diffr. **20**, 43 (2005).
[3] M. C. Stennett, G. C. Miles, J. Sharman, I. M. Reaney, and A. R. West, J. Eur. Ceram. Soc. **25**, 2471 (2005).
[4] G. C. Miles, M. C. Stennett, I. M. Reaney, and A. R. West, J. Mater. Chem. **15**, 798 (2005).
[5] M. Stennett, I. M. Reaney, G. C. Miles, D. I. Woodward, A. R. West, C. A. Kirk, and I. Levin, J. Appl. Phys. **101**, 104114 (2007).
[6] S. Kamba, S. Veljko, M. Kempa, M. Savinov, V. Bovtun, P. Vanek, J. Petzelt, M. C. Stennett, I. M. Reaney, and A. R. West, J. Eur. Ceram. Soc. **25**, 3069 (2005).
[7] M. C. Stennett, I. M. Reaney, G. C. Miles, and A. R. West, J. Am. Ceram. Soc. **90**, 980 (2007).
[8] I. Levin, M. C. Stennett, G. C. Miles, D. I. Woodward, A. R. West, and I. M. Reaney, Appl. Phys. Lett. **89**, 122908 (2006).
[9] P. B. Jamieson, S. C. Abrahams, and J. L. Bernstein, J. Chem. Phys. **50**, 4352 (1969).
[10] P. Labbe, H. Leligny, B. Raveau, J. Scheck, and J. C. Toledano, J. Phys. C **2**, 25 (1986).
[11] J. C. Toledano and J. Schneck, Solid State Commun. **16**, 1101 (1975).
[12] P. B. Jamieson, S. C. Abrahams, and J. L. Bernstein, J. Chem. Phys. **48**, 5048 (1968).
[13] L. A. Bursill and P. J. Lin, Acta Crystallogr., Sect. B: Struct. Sci. **43**, 49 (1987).
[14] H. Beltrán, E. Cordoncillo, P. Escribano, D. C. Sinclair, and A. R. West, J. Am. Ceram. Soc. **87**, 2132 (2004).
[15] M. R. Suchomel and P. K. Davies, Appl. Phys. Lett. **86**, 262905 (2005).
[16] T. Bongkarn, G. Rujijanagul, and S. J. Milne, Appl. Phys. Lett. **92**, 092905 (2008).